

# 1 Seasonal and interannual variabilities of the barrier layer 2 thickness in the tropical Indian Ocean

3 Xu Yuan\*<sup>1</sup>, Xiaolong Yu<sup>2</sup>, Zhongbo Su<sup>1</sup>,

- 4 1. Faculty of Geo-Information Science and Earth Observation (ITC), University of  
5 Twente, the Netherlands
- 6 2. State Key Laboratory of Marine Environmental Science, College of Ocean and Earth  
7 Sciences, Xiamen University, Xiamen 361101, China

8 \*Correspondence to: Xu Yuan (x.yuan@utwente.nl)

9 **Abstract.** The seasonal and interannual variations of the barrier layer thickness (BLT) in the tropical Indian  
10 Ocean (TIO) is investigated in this study using the Simple Ocean Data Assimilation version 3 (SODA v3) ocean  
11 reanalysis dataset. Analysis of this study suggests energetic but divergent seasonal variabilities of BLT in the  
12 western TIO (55°E-75°E, 5°N -12°S) and the eastern TIO (85°E-100°E, 5°N -12°S). For instance, the thinner  
13 barrier layer (BL) is observed in the western TIO during boreal winter as a result of decreasing sea surface  
14 salinity (SSS) and shallower thermocline, which are associated with the intrusion of freshwater flux and the  
15 wind-induced downwelling, respectively. On the contrary, the variation of BLT in the eastern TIO mainly  
16 corresponds to the thermocline in all seasons. The interannual variability of BLT is explored with Indian Ocean  
17 Dipole (IOD) and El Niño Southern Oscillation (ENSO). During the mature phase of the positive IOD events,  
18 thinner BL in the eastern TIO is attributed to the shallower thermocline, while thicker BL appears in the western  
19 TIO due to deeper thermocline and fresher surface water. During the negative IOD events, thicker BL only  
20 occurs in the eastern TIO corresponding to the deeper thermocline. During the ENSO events, prominent BLT  
21 patterns are observed in the western TIO corresponding to two different physical processes during the  
22 developing and decaying phase of the El Niño events. During the developing phase of El Niño events, thicker  
23 BL in the western TIO is associated with deepening thermocline induced by the westward Rossby wave. During  
24 the decaying phase of El Niño events, the thermocline is weakly deepening while the BLT reaches its maxima  
25 induced by the decreasing SSS.

## 26 1 Introduction

27 The upper-ocean traditionally included only the mixed layer and the thermocline. The terminology barrier layer  
28 (BL), was recently raised as the mixed layer depth (MLD) was redefined from using the temperature (de Boyer  
29 Montégut et al., 2004) to using the oceanic density (Kara et al., 2000; Mignot et al., 2007). The barrier layer  
30 thickness (BLT) is simply the depth between the bottom of the mixed layer defined by density, and the top of the  
31 thermocline (Lukas and Lindstrom, 1991; Masson et al., 2002; Sprintall and Tomczak, 1992). Although BL is  
32 much thinner than the other two layers, it plays a key role in oceanic dynamics and air-sea interaction. For  
33 example, BL helps to sustain the heat in the mixed layer by isolating the temperature in the upper ocean from the  
34 cooling entrainment. Accordingly, BL is crucial in the formation of the El Niño Southern Oscillation (ENSO)  
35 and contributes to the formation of the different ENSO types (conventional ENSO and ENSO Modoki) (Singh et  
36 al., 2011; Maes, 2002; Maes et al., 2006; Maes et al., 2005). Also, the spatial structure of BLT led by different

37 Ekman drift is crucial for the formation of monsoon cyclones in the pre-monsoon season (Thadathil et al., 2007;  
38 Vinayachandran et al., 2002; Masson et al., 2005; Neetu et al., 2012).

39 The variability of BLT is mainly affected by the change of MLD and thermocline due to various mechanisms,  
40 such as heavy precipitation, oceanic currents, wind stress, and oceanic waves (Bosc et al., 2009; Mignot et al.,  
41 2007; Masson et al., 2002; Qu and Meyers, 2005). For instance, thicker BL mainly presents in the areas beneath  
42 the Intertropical Convergence Zone (ITCZ) with decreasing SSS due to abundant rainfall (Vialard and Delecluse,  
43 1998) or large river discharge (Pailler et al., 1999). The strong wind stress anomalies could also contribute to  
44 thickening the BL via deepening the thermocline (Seo et al., 2009).

45 Compared to the tropical Pacific and the Atlantic Ocean, the tropical Indian Ocean (TIO) is characterized with a  
46 shallower thermocline in the west (Yokoi et al., 2012, 2008; Yu et al., 2005) and stronger interannual variation  
47 of upper-ocean temperature in the east (Li et al., 2003; Saji et al., 1999), which provides a unique region to  
48 evaluate the seasonal and interannual variabilities of BLT.

49 The strong seasonality of BLT has been observed in some subregions of the TIO, such as the southeastern  
50 Arabian Sea, the Bay of Bengal, and the southeastern TIO (Schott et al., 2009). These regions are also  
51 characterized by the strong seasonality of SSS due to different hydrological processes (Rao, 2003;  
52 Subrahmanyam et al., 2011; Zhang et al., 2016; Zhang and Du, 2012). Overall, the seasonality of BLT in the  
53 TIO is partly consistent with the change of SSS due to the impact of freshwater (Masson et al., 2002; Qu and  
54 Meyers, 2005).

55 The interannual variability of BLT in the southeastern TIO could be partly explained by IOD events (Qiu et al.,  
56 2012). During the positive IOD year (*e.g.*, 2006), thinner BL in the southeastern TIO is mainly led by the  
57 shallower thermocline induced by the upwelling Kelvin wave in the presence of weakly shoaling MLD. In the  
58 negative IOD year (*e.g.*, 2010), a thicker BL is expected due to the extending of the thermocline. Furthermore, at  
59 the sub-seasonal scale, the zonal SSS gradient driven by the freshwater advection results in a thicker BL to  
60 sustain a fresh and stable MLD (Drushka et al., 2014).

61 Existing studies on the interannual variability of BLT were mainly focused on specific years and lacking long-  
62 term evaluation. More importantly, the interannual variability of both thermocline and SSS are supposed to be  
63 associated with the ENSO events (Grunseich et al., 2011; Rao and Sivakumar, 2003; Subrahmanyam et al., 2011;  
64 Zhang et al., 2013), but relationships between BLT and ENSO are scarcely reported in the TIO. Also, the relative  
65 impact of SSS and thermocline depth on the variability of BLT and SSS variation is still unclear and is not  
66 systematically investigated in the TIO. Thus, the evolution of the seasonal and interannual variabilities of BLT  
67 and its relationship with SSS and thermocline anomalies are still highly desired. The Simple Ocean Data  
68 Assimilation (SODA) version 3 ocean reanalysis dataset covers time-series data from 1980 to 2015, which could  
69 be adequate for such purpose.

70 The remainder of this paper is arranged as follows. In Section 2, we briefly describe the datasets and methods.  
71 Comparisons of the BLT variability interpreted from both observed and reanalysis datasets in the TIO is  
72 presented in Section 3. Section 4 presents the seasonal variability of the BLT in the TIO, while its interannual  
73 variability is shown in Section 5. At last, summary and discussions are given in Section 6.

## 74 2 Data and Methods

75 Two datasets are used in this study to investigate the variability of BLT in the TIO. The first one is the monthly  
76 global gridded observation and reanalysis products with 1° horizontal resolution from 2005 to 2015, which is  
77 compiled from Argo profiles products provided by the French Research Institute for Exploration of the Sea  
78 (Ifremer: [http://www.ifremer.fr/cerweb/deboyer/mld/Subsurface Barrier Layer Thickness.php](http://www.ifremer.fr/cerweb/deboyer/mld/Subsurface_Barrier_Layer_Thickness.php)). BLT is  
79 calculated as the difference between  $TTD_{DTm02}$  and  $MLD$ .

$$80 \quad BLT = TTD_{DTm02} - MLD$$

81 where  $TTD_{DTm02}$  is the depth at the top of thermocline, which is defined as the depth at which the  
82 surface temperature is cooled by 0.2 °C than sea surface temperature and hereafter referred to as the isothermal  
83 layer depth (ILD).  $MLD$  is the mixed layer depth defined by oceanic density at which depth the density is 0.03  
84 kg/m<sup>3</sup> larger than that of the surface (de Boyer Montégut et al., 2007; Mignot et al., 2007).

85 Another dataset is the latest released SODA version 3 reanalysis data (1980-2015) with a horizontal resolution of  
86 0.5°, which is hereafter denoted as SODA v3 data and can be accessed from the Asia-Pacific Data-Research  
87 Center (APDRC: [http://apdrc.soest.hawaii.edu/datadoc/soda\\_3.3.1.php](http://apdrc.soest.hawaii.edu/datadoc/soda_3.3.1.php)). SODA v3 has reduced systematic errors  
88 in the upper ocean and has improved the accuracy of the poleward variability in the tropic (Carton et al., 2018).  
89 It has 26 vertical levels with a 15 m resolution near the sea surface. We adopted the same Ifremer equation to  
90 calculate SODA BLT as the difference between density and temperature defined MLD.

91 Salinity and temperature in the first level (5m) are adopted as the SODA SSS and sea surface temperature (SST),  
92 respectively. The thermocline depth is defined as the depth of the 20 °C isotherms.

93 Monthly SST between 1980 and 2015 on a grid of 1°x1° is acquired from Hadley Center Global Sea Ice and Sea  
94 Surface Temperature (HadISST: <https://climatedataguide.ucar.edu/climate-data/sst-data-hadisst-v11>) to calculate  
95 the Nino3.4 index. The Nino3.4 index is the average SST anomaly in the area of (5°N -5°S, 170°W -120°W).

96 The simultaneous and lead-lag correlations are evaluated in this study with the  $t$ -student significance test. In all  
97 the datasets, we removed the annual cycle of each parameter before the interannual correlation analysis. The  
98 composition analysis is also employed to evaluate the interannual variability of BLT using the Monte-Carlo  
99 significance test. The process of Monte-Carlo is that the IOD/El Niño/La Nina years are randomly shuffled (10  
100 000 times) for each month, and a mean  $t$ -student significance test is used to calculate the  $t$  statistic for the  
101 selected areas. The mean of the  $t$  statistic generated by the random simulations exceeding that of the actual  $t$   
102 value is determined and assessed at the 5% significance level. The positive and negative IOD years are provided  
103 by the Bureau of Meteorology (<http://www.bom.gov.au/climate/iod/>), and the El Niño and La Nina years are  
104 obtained from Golden weather gate service (<https://ggweather.com/enso/oni.htm>). Monthly mean values are  
105 averaged over a three-sequential month for different seasons, e.g., December-January-February (DJF) for boreal  
106 winter, March-April-May (MAM) for boreal spring, June-July-August (JJA) for boreal summer and September-  
107 October-November (SON) for boreal autumn. All the area-averaged parameters shown in this study are weighted  
108 by the cosine of the latitude.

### 109 3 BLT in the Indian Ocean

110 BLT in the TIO calculated from SODA v3 is first validated against Argo float observation from 2005 to 2015.  
111 As shown in Figure 1, the seasonal BLT climatology obtained from SODA v3 is biased thinner in the Bay of  
112 Bengal in all seasons compared to that derived from Argo. This thinner BL in SODA v3 is probably because it  
113 lacks the runoff data from the Bay of Bengal as input in its reanalysis (Carton et al., 2018; Carton and Giese,  
114 2008, 2006). Additionally, SODA BLT fails to capture the BLT feature on the west coast of Africa and the  
115 northwestern Arabian Sea (see the white areas right to green line), where no BLT is expected due to the salinity  
116 inversion. However, for the area of interest in the TIO (55°E-100°E, 5°N -12°S), the BLT in SODA v3 shows a  
117 coherent spatial pattern with the Argo BLT, where BL is, in general, thicker in the east and thinner in the west.  
118 The seasonal evolution of BLT in the east obtained from SODA is consistent with that from Argo, shown as a  
119 decreasing trend from boreal winter to spring and an increasing trend from boreal summer to autumn.

120 Two sub-regions are highlighted to evaluate the seasonal and interannual variabilities of SODA BLT, namely  
121 western TIO (55°E-75°E, 5°N -12°S) and eastern TIO (85°E-100°E, 5°N -12°S). Because these two sub-regions  
122 not only represent the zonal difference of the BLT in the TIO but also include the well-known areas of  
123 Seychelles Chicago Thermocline Ridge [SCTR, (60°E-75°E, 12°S-5°S)] and the eastern IOD area [IODE,  
124 (90°E-100°E, 10°S-EQ)] (Manola et al., 2015; Yokoi et al., 2012, 2008). As shown in Figure 2, region-averaged  
125 BLT obtained from SODA v3 in the western TIO is greater than that of Argo, especially during boreal summer  
126 and autumn. In the eastern TIO, SODA v3 BLT is quite comparable with that of Argo, except for slight  
127 discrepancies in June and July. The trend of BLT seasonality obtained from SODA v3 and Argo are, however,  
128 overall consistent, suggesting the robustness of using SODA v3 data in interpreting the BLT variabilities in the  
129 TIO.

130 Due to the insufficient temperature-salinity observations, we only compare the interannual variability of the  
131 SODA v3 BLT with the Argo between 2005 and 2010. As shown in Figure 3, the interannual variability of BLT  
132 from SODA v3 and Argo is very consistent in both the western and eastern TIO. The correlation coefficients  
133 between SODA v3 and Argo for the western and eastern TIO are 0.75 and 0.90, respectively. Results in Figure 3  
134 confirm that SODA v3 is adequate to evaluate the long-term seasonal and interannual variabilities of the BLT in  
135 the TIO.

136 The seasonal and interannual variations of MLD and ILD averaged over the western and eastern TIO are also  
137 presented in Figure 4 to investigate the dominant driver for the BLT variability. Overall, the seasonal  
138 variabilities of MLD and ILD present a consistent annual cycle in both subregions. The seasonality of BLT,  
139 however, exerts discrepancies between these two regions (Figures 4a and 4b). Specifically, a semi-annual cycle  
140 of BLT is observed in the western TIO, compared to an annual cycle of BLT observed in the eastern TIO. The  
141 interannual variabilities of BLT are also different in the western and eastern TIO (Figure 4c and 4d). In the  
142 western TIO, the interannual variability of BLT is more related to the ILD variation. For example, the years with  
143 thicker BL in the western are associated with deeper ILD, such as 1982, 1983, 1991, and 1996. On the contrary,  
144 in the eastern TIO, the relative impact of MLD and ILD on the interannual variability of BLT cannot be  
145 discriminated. For instance, deeper BLT occurs in 1981, 1985, and 1996 corresponding to relatively shallower  
146 MLD, while the other years of deeper BLT, such as 1994, 1999, and 2001, are associated with deeper ILD.  
147 Additionally, the interannual correlation coefficients between BLT and MLD are -0.07 and -0.25 for the western

148 and eastern TIO, respectively, and the correlations coefficients between BLT and ILD are 0.47 and 0.38 in those  
149 two sub-regions. The low correlation coefficients suggest that neither MLD nor ILD can fully explain the BLT  
150 variabilities in the TIO. Therefore, the difference of BLT variabilities in the western and eastern TIO needs to be  
151 further explained. In the subsequent analysis, the variables in MLD, including SST and SSS, and the thermocline  
152 are selected to explain the BLT variabilities in the TIO.

#### 153 **4 Seasonal variation**

154 It is well known that the area with the thickest BL in the TIO corresponds to freshest surface water, while the  
155 areas of the thinnest BL corresponds to saltiest surface water (Agarwal et al., 2012; Felton et al., 2014; Han and  
156 McCreary, 2001; Vinayachandran and Nanjundiah, 2009). The spatial feature between BLT and SSS in different  
157 seasons are presented in Figure 5, where the seasonality of SSS and BLT does not co-vary, especially near the  
158 equator. For example, surface saltier water in the western TIO elongates eastward during boreal winter and  
159 spring and retreats during boreal summer and autumn, while BLT does not vary accordingly. In the eastern TIO,  
160 BLT presents a more prominent seasonality than that of SSS, with a maximum in boreal autumn.

161 Figure 6 shows the in-phase correlations of SST and SSS anomalies with BLT anomalies. Here, the SSS, SST  
162 and BLT anomalies have been averaged as the functions of longitude vs. time in the western and eastern TIO,  
163 respectively. The seasonal BLT-SST relationship in the western TIO is not robust as only a few areas exceed the  
164 95% significance level (see Figure 6a). A short-term (less than two months) negative correlation between BLT  
165 and SST anomalies can be observed in the eastern TIO during boreal winter. This negative BLT-SST correlation  
166 also exists when the HadISST data is employed (figure not shown). Compared with the seasonal BLT-SST  
167 relationship, the seasonal BLT-SSS relationship is more prominent in the TIO, especially in the western TIO  
168 (Figure 6b). This negative correlation between BLT and SSS starts from January and extends to June.

169 To further understand the seasonal relationship of BLT with SSS and thermocline, we adopt the lead-lag crossing  
170 correlation analysis for BLT anomalies with respect to SSS and the thermocline depth anomalies in January  
171 (JAN), April (APR), July (JUL) and October (OCT). The significant area of the lead-lag negative correlation  
172 between SSS and BLT mainly locates in the western TIO (Figures 7a-d), which is consistent with that of their in-  
173 phase correlation (Figure 6b). During boreal winter, spring, and autumn, the variation of SSS could affect BLT  
174 variability in the next two months (Figures 7a and 7d). For example, fresher (saltier) water in October in the  
175 western TIO could lead to thicker (thinner) BL in November and December. The positive correlation between  
176 BLT and the thermocline depth is much prominent in the western TIO, particularly in January. The variation of  
177 the thermocline in January has an impact on BLT variations up to the next four months (Figure 7e). During  
178 boreal autumn, a strong BLT-thermocline correlation mainly occurs in the eastern TIO. The variation of the  
179 thermocline in October could have an impact on BLT variations in the three successive months (Figure 7h).

180 We also examined the corresponding atmospheric forcing in the western and eastern TIO. Figure 8 shows the  
181 seasonal evolution of the upper-ocean salinity, MLD, ILD, the thermocline depth, the freshwater flux  
182 (Precipitation minus Evaporation, P-E), and the zonal component of the wind stress. In the western TIO,  
183 freshening of the upper-ocean water from October to April is observed due to freshwater flux, which in turn,  
184 thickens the BL, consistent with the analysis in Figure 6b. In the meantime, westerlies lead to Ekman pumping in  
185 the western TIO, resulting in the thicker thermocline depth (green line) from December to April, which in turn,

186 also makes the BL thicker. Driving factors of the BLT seasonality in the eastern TIO are more complex than that  
187 in the western TIO. Firstly, the seasonal evolution of SSS has a semi-annual feature, while THE freshwater flux  
188 does not. This can be explained by the Indonesian throughflow, which brings freshwater from the Pacific Ocean  
189 into the eastern TIO (Shinoda et al., 2012). Secondly, the thermocline presents the opposite seasonal cycle  
190 compared with that in the western TIO. However, the zonal wind stress displays a similar seasonal variation in  
191 both the western and eastern TIO. Last but not least, the salinity in the deeper ocean varies similarly to the  
192 thermocline in the eastern TIO, which is not observed in the western TIO. Thus, the freshwater flux and the  
193 wind-driven upwelling cannot fully explain the BLT seasonality in the eastern TIO. Felton et al. (2014) have  
194 suggested that the seasonal BLT variation in the eastern TIO may be related to the sea level and ILD oscillation.

## 195 **5 Interannual Variation**

196 IOD, as the zonal SST gradients along the equatorial TIO, is a crucial climate mode on the interannual scale  
197 (Schott et al., 2009). IOD events mostly develop and mature within boreal autumn and decay in boreal winter  
198 (Saji et al., 1999). It corresponds well with local precipitation and wind change and has an impact on the SSS  
199 (Saji and Yamagata, 2003a). The intensity of IOD could be defined by the Dipole Mode Index (DMI), which is  
200 the difference between SST anomalies in the region of (10°S –10°N, 50°E-70°E) and (10°S –EQ, 90°E-110°E)  
201 (Saji et al., 1999). Based on the DMI, we composited the monthly SSS, BLT, and the thermocline depth  
202 anomalies for positive IOD (pIOD) and negative IOD (nIOD) events, respectively. The corresponding years are  
203 listed in Table 1. Figure 9 presents the composited seasonal variations for our current dataset during the period of  
204 1980-2015. The Monte-Carlo procedure has been used to evaluate the significance of the composite variations  
205 (green shaded areas). If the value of the variables exceeds the green shaded areas, it is assessed significant at the  
206 95% significance level. In the eastern TIO (Figures 9a, 9c, and 9e), there are no prominent patterns of SSS  
207 during the negative (positive) IOD events. This is because the eastward (westward) saltier (fresher) water  
208 advection can compensate for the reduced (increased) precipitation due to the presence of the strong Wyrтки jet  
209 (Thompson et al., 2006). In contrast, the thermocline and BLT display a prominent seasonal phase locking  
210 feature in the eastern TIO. Specifically, during the mature and decaying phases of the positive IOD events,  
211 shallower thermocline depth due to strong upwelling leads to thinner BL. This thinner BL provides favorable  
212 circumstances for the cold water intrusion into the ocean surface, which contributes to the intensification of the  
213 positive IOD events (Deshpande et al., 2014). During the mature phase of the negative IOD events, deeper  
214 thermocline along with a thicker BL could be observed in the eastern TIO due to the strong downwelling. In the  
215 western TIO (Figures 9b, 9d, and 9f), the thicker BL prominently occurs only during the mature phase of the  
216 positive IOD events that are associated with deeper thermocline and fresher surface water, which are attributed  
217 due to the wind-induced downwelling and the westward freshwater advection, respectively.

218 In previous studies, a significant seasonal phase-locking impact of ENSO on the TIO has been addressed (Schott  
219 et al., 2009; Zhang and Yang, 2007). This seasonal phase-locking impact mainly exists during the developing  
220 phase of ENSO (boreal autumn), the mature phase of ENSO (boreal winter), and the decaying phase of ENSO  
221 (boreal spring) in different areas of the TIO. We composited our variables based on the ENSO events from Table  
222 2. Figure 10 presents the composited results of the seasonal variation of BLT, SSS, and thermocline. The thinner  
223 BL is mainly associated with shallower thermocline during the developing and mature phases of El Niño  
224 (Figures 10c and 10e), which can be explained by the anomalous easterlies along the equator invoked by the

225 adjusted Walker Circulation (Alexander et al., 2002; Kug and Kang, 2006). In the western TIO, thicker BL  
226 presents two peaks during the developing and decaying phase of El Niño events (Figure 10d). The first peak of  
227 thicker BLT corresponds to a peak of deepening thermocline depth due to the westward downwelling Rossby  
228 wave and the anomalous wind stress induced by El Niño (Kug and Kang, 2006; Xie et al., 2002). The second  
229 peak of thicker BL is more significant, which connects to the peak of the deepening thermocline and decreasing  
230 SSS (Figures 10b and 10f).

231 The pattern of BLT in the western TIO during the El Niño events is the most prominent, and its two peaks can be  
232 explained by two physical mechanisms. Thus, we calculate the lead-lag correlations between BLT, thermocline  
233 and SSS anomalies and the Nino3.4 index from 1980 to 2015 to investigate the BLT-El Niño relationship. The  
234 correlation coefficients between the thermocline depth anomalies and the Nino3.4 index reach the significant  
235 values during the mature period of El Niño (Figure 11b). Also, the correlation between thermocline and Nino3.4  
236 index shows a time delay that is longitude dependent, which is consistent with the result of Xie et al., (2002).  
237 This deeper thermocline due to the westward downwelling Rossby wave induced by El Niño affects the  
238 corresponding BL. As shown in Figure 11a, a remarkably positive correlation between BLT and the Nino3.4  
239 index is one month apart. Then, the correlation between the thermocline depth anomalies and El Niño becomes  
240 weaker during the decaying period of El Niño (Figure 11b). However, there is an enlarged correlation between  
241 BLT and ENSO. This enlarged pattern accompanies with the appearance of a negative correlation between SSS  
242 and ENSO (Figure 11c). The negative SSS anomalies due to precipitation induced by El Niño via the adjusting  
243 Walker circulation and the westward Rossby wave in the western TIO thicken the BLT anomalies (Figures 11d  
244 and 11e).

245 To further verify the impact of IOD and ENSO events on the interannual variation of BLT, the time series of  
246 BLT, SSS, and thermocline anomalies averaged over the western TIO during boreal winter and spring from 1980  
247 to 2015 are shown in Figure 12. During boreal winter (Figure 12a), thicker BL and deeper thermocline could be  
248 found in 1983, 1992, 1998, corresponding to the mature phase of El Niño events (Table 2). During boreal spring  
249 (Figure 12b), thicker BL and deeper thermocline could also be observed in the decaying phase of El Niño events,  
250 accompanied with fresher surface water. On the other hand, the effect of IOD on the interannual variability of  
251 BLT could be observed in specific years as well, such as 1983,1998, and 2006 (Table 1).

## 252 **6 Summary**

253 The seasonal and interannual variabilities of BLT in the TIO are investigated by using the SODA v3 ocean  
254 reanalysis dataset. SODA v3 reasonably well reproduces the observed mean and variabilities of BLT in the TIO  
255 when compared to Argo.

256 The dominant contributors to the BLT seasonality are different in the western and eastern TIO. BLT in the eastern  
257 TIO is positively correlated to the thermocline depth during boreal autumn, winter and spring, and the positive  
258 impact could last for the next three to four months. On the contrary, BLT in the western TIO is negatively correlated  
259 to SSS during boreal winter, spring, and autumn. The change of SSS can further control BLT variation in up to  
260 two subsequent months. Additionally, the change of BLT in the western TIO during boreal winter could also be  
261 affected by the variation of the thermocline depth. For instance, during boreal winter, fresher surface water and

262 shallower thermocline depth result in thinner BL in the western TIO, which is due to freshwater flux and strong  
263 wind convergence induced by both the winter monsoon wind and the south-easterlies (Yokoi et al., 2012).

264 The interannual variability of BLT exerts a seasonal phase locking pattern during the IOD and ENSO years. In  
265 the eastern TIO, thicker BL is led by the deeper thermocline due to wind-induced downwelling during the  
266 mature phase of the negative IOD events. In contrast, thinner BL is dominated by the shallower thermocline due  
267 to wind-induced upwelling during the developing and mature phases of the positive IOD events. In the western  
268 TIO, the thicker BL is only observed during the mature and decaying phases of the positive IOD events, along  
269 with deeper thermocline and fresher surface water.

270 The prominent patterns of BLT in the western TIO can only be detected during the El Niño events. According to  
271 the theory of Xie et al. (2002), there is warmer water developing in the eastern tropical Pacific Ocean (El Niño),  
272 resulting in the anomalous easterlies and invoking the downwelling Rossby wave along the equatorial TIO.  
273 Thereby, the thermocline depth has been deepened in the western TIO, resulting in the thicker BL. This  
274 thickening BL hampers the upwelling process and helps to sustain warmer SST. During the decaying phase of El  
275 Niño events, there is an anomalous ascending branch of the adjusted Walker circulation in the western TIO. As a  
276 result, SSS in the western TIO is decreasing due to abundant precipitation. Consequently, fresher surface water  
277 contributes to thickening BL, which in turn, sustains the warmer SST in the western TIO.

## 278 **Acknowledgment**

279 We thank Dr. A.J. George Nurser and one anonymous reviewer for their constructive comments to improve the  
280 manuscript. The use of the following datasets is gratefully acknowledged: the grided ocean parameter datasets are  
281 available at the Asian-Pacific Data-Research Center (<http://apdrc.soest.hawaii.edu/data/data.php>) and National  
282 Oceanic and Atmospheric Administration (<https://www.esrl.noaa.gov/psd/data/gridded/data.noaa.oisst.v2.html>).

## 283 **References**

- 284 Agarwal, N., Sharma, R., Parekh, A., Basu, S., Sarkar, A., and Agarwal, V. K.: Argo observations of barrier layer in  
285 the tropical Indian Ocean, *Advances in Space Research*, 50, 642-654, 2012.
- 286 Alexander, M. A., Bladé, I., Newman, M., Lanzante, J. R., Lau, N.-C., and Scott, J. D.: The atmospheric bridge:  
287 The influence of ENSO teleconnections on air–sea interaction over the global oceans, *Journal of Climate*, 15,  
288 2205-2231, 2002.
- 289 Bosc, C., Delcroix, T., and Maes, C.: Barrier layer variability in the western Pacific warm pool from 2000 to 2007,  
290 *Journal of Geophysical Research: Oceans*, 114, 2009.
- 291 Carton, J. A., Chepurin, G. A., and Chen, L.: SODA3: a new ocean climate reanalysis, *Journal of Climate*, 31,6967-  
292 6983, 2018.
- 293 Carton, J. A. and Giese, B. S.: A reanalysis of ocean climate using Simple Ocean Data Assimilation (SODA),  
294 *Monthly Weather Review*, 136, 2999-3017, 2008.
- 295 Carton, J. A. and Giese, B. S.: SODA: A reanalysis of ocean climate, submitted to *Monthly Weather Review*,  
296 2005.
- 297 Chowdary, J., Gnanaseelan, C., and Xie, S.: Westward propagation of barrier layer formation in the 2006–07  
298 Rossby wave event over the tropical southwest Indian Ocean, *Geophysical Research Letters*, 36, 2009.
- 299 de Boyer Montégut, C., Madec, G., Fischer, A. S., Lazar, A., and Iudicone, D.: Mixed layer depth over the global  
300 ocean: An examination of profile data and a profile–based climatology, *Journal of Geophysical Research:*  
301 *Oceans*, 109, 2004.
- 302 de Boyer Montégut, C., Mignot, J., Lazar, A., and Cravatte, S.: Control of salinity on the mixed layer depth in the  
303 world ocean: 1. General description, *Journal of Geophysical Research: Oceans*, 112, 2007.



304 Deshpande, A., Chowdary, J., and Gnanaseelan, C.: Role of thermocline-SST coupling in the evolution of IOD  
305 events and their regional impacts, *Climate dynamics*, 43, 2014.

306 Drushka, K., Sprintall, J., and Gille, S. T.: Subseasonal variations in salinity and barrier-layer thickness in the  
307 eastern equatorial Indian Ocean, *Journal of Geophysical Research: Oceans*, 119, 805-823, 2014.

308 Felton, C. S., Subrahmanyam, B., Murty, V., and Shriver, J. F.: Estimation of the barrier layer thickness in the  
309 Indian Ocean using Aquarius Salinity, *Journal of Geophysical Research: Oceans*, 119, 4200-4213, 2014.

310 Grunseich, G., Subrahmanyam, B., Murty, V., and Giese, B. S.: Sea surface salinity variability during the Indian  
311 Ocean Dipole and ENSO events in the tropical Indian Ocean, *Journal of Geophysical Research: Oceans* (1978–  
312 2012), 116, 2011.

313 Han, W. and McCreary, J. P.: Modeling salinity distributions in the Indian Ocean, *Journal of Geophysical  
314 Research*, 106, 859-877, 2001.

315 Kara, A. B., Rochford, P. A., and Hurlburt, H. E.: An optimal definition for ocean mixed layer depth, *Journal of  
316 Geophysical Research: Oceans* (1978–2012), 105, 16803-16821, 2000.

317 Kug, J.-S. and Kang, I.-S.: Interactive feedback between ENSO and the Indian Ocean, *Journal of climate*, 19,  
318 1784-1801, 2006.

319 Li, T., Wang, B., Chang, C., and Zhang, Y.: A theory for the Indian Ocean dipole–zonal mode, *Journal of the  
320 Atmospheric Sciences*, 60, 2119-2135, 2003.

321 Lukas, R. and Lindstrom, E.: The mixed layer of the western equatorial Pacific Ocean, *Journal of Geophysical  
322 Research: Oceans*, 96, 3343-3357, 1991.

323 Maes, C.: Salinity barrier layer and onset of El Niño in a Pacific coupled model, *Geophysical Research Letters*,  
324 29, 2002.

325 Maes, C., Ando, K., Delcroix, T., Kessler, W. S., McPhaden, M. J., and Roemmich, D.: Observed correlation of  
326 surface salinity, temperature and barrier layer at the eastern edge of the western Pacific warm pool,  
327 *Geophysical Research Letters*, 33, 2006.

328 Maes, C., Picaut, J., and Belamari, S.: Importance of the salinity barrier layer for the buildup of El Niño, *Journal  
329 of climate*, 18, 104-118, 2005.

330 Manola, I., Selten, F., de Ruijter, W., and Hazeleger, W.: The ocean-atmosphere response to wind-induced  
331 thermocline changes in the tropical South Western Indian Ocean, *Climate Dynamics*, 45, 989-1007, 2015.

332 Masson, S., Delecluse, P., Boulanger, J. P., and Menkes, C.: A model study of the seasonal variability and  
333 formation mechanisms of the barrier layer in the eastern equatorial Indian Ocean, *Journal of Geophysical  
334 Research: Oceans*, 107, SRF 18-11-SRF 18-20, 2002.

335 Masson, S., Luo, J. J., Madec, G., Vialard, J., Durand, F., Gualdi, S., Guilyardi, E., Behera, S., Delécluse, P., and  
336 Navarra, A.: Impact of barrier layer on winter–spring variability of the southeastern Arabian Sea, *Geophysical  
337 research letters*, 32, 2005.

338 Mignot, J., de Boyer Montégut, C., Lazar, A., and Cravatte, S.: Control of salinity on the mixed layer depth in the  
339 world ocean: 2. Tropical areas, *Journal of Geophysical Research: Oceans*, 112, 2007.

340 Neetu, S., Lengaigne, M., Vincent, E. M., Vialard, J., Madec, G., Samson, G., Ramesh Kumar, M., and Durand, F.:  
341 Influence of upper-ocean stratification on tropical cyclone-induced surface cooling in the Bay of Bengal,  
342 *Journal of Geophysical Research: Oceans*, 117, 2012.

343 Pailler, K., Bourlès, B., and Gouriou, Y.: The barrier layer in the western tropical Atlantic Ocean, *Geophysical  
344 Research Letters*, 26, 2069-2072, 1999.

345 Qiu, Y., Cai, W., Li, L., and Guo, X.: Argo profiles variability of barrier layer in the tropical Indian Ocean and its  
346 relationship with the Indian Ocean Dipole, *Geophysical Research Letters*, 39, 2012.

347 Qu, T. and Meyers, G.: Seasonal variation of barrier layer in the southeastern tropical Indian Ocean, *Journal of  
348 Geophysical Research: Oceans*, 110, 2005.

349 Rao, R. and Sivakumar, R.: Seasonal variability of sea surface salinity and salt budget of the mixed layer of the  
350 north Indian Ocean, *Journal of Geophysical Research: Oceans* (1978–2012), 108, 9-1-9-14, 2003.

351 Rao, R. R.: Seasonal variability of sea surface salinity and salt budget of the mixed layer of the north Indian  
352 Ocean, *Journal of Geophysical Research*, 108, 2003.

353 Saji, N., Goswami, B. N., Vinayachandran, P., and Yamagata, T.: A dipole mode in the tropical Indian Ocean,  
354 *Nature*, 401, 360-363, 1999.

355 Schott, F. A., Xie, S. P., and McCreary, J. P.: Indian Ocean circulation and climate variability, *Reviews of  
356 Geophysics*, 47, 2009.

357 Seo, H., Xie, S.-P., Murtugudde, R., Jochum, M., and Miller, A. J.: Seasonal effects of Indian Ocean freshwater  
358 forcing in a regional coupled model, *Journal of Climate*, 22, 6577-6596, 2009.

359 Shinoda, T., Han, W., Metzger, E. J., and Hurlburt, H. E.: Seasonal variation of the Indonesian throughflow in  
360 Makassar Strait, *Journal of Physical Oceanography*, 42, 1099-1123, 2012.

361 Singh, A., Delcroix, T., and Cravatte, S.: Contrasting the flavors of El Niño–Southern Oscillation using sea surface  
362 salinity observations, *Journal of Geophysical Research: Oceans*, 116, 2011.

363 Sprintall, J. and Tomczak, M.: Evidence of the barrier layer in the surface layer of the tropics, *Journal of*  
364 *Geophysical Research: Oceans*, 97, 7305-7316, 1992.

365 Subrahmanyam, B., Murty, V., and Heffner, D. M.: Sea surface salinity variability in the tropical Indian Ocean,  
366 *Remote Sensing of Environment*, 115, 944-956, 2011.

367 Thadathil, P., Muraleedharan, P., Rao, R., Somayajulu, Y., Reddy, G., and Revichandran, C.: Observed seasonal  
368 variability of barrier layer in the Bay of Bengal, *Journal of Geophysical Research: Oceans*, 112, 2007.

369 Thompson, B., Gnanaseelan, C., and Salvekar, P.: Variability in the Indian Ocean circulation and salinity and its  
370 impact on SST anomalies during dipole events, *Journal of Marine Research*, 64, 853-880, 2006.

371 Vialard, J. and Delecluse, P.: An OGCM study for the TOGA decade. Part II: Barrier-layer formation and  
372 variability, *Journal of physical oceanography*, 28, 1089-1106, 1998.

373 Vinayachandran, P., Murty, V., and Ramesh Babu, V.: Observations of barrier layer formation in the Bay of  
374 Bengal during summer monsoon, *Journal of Geophysical Research: Oceans*, 107, SRF 19-11-SRF 19-19, 2002.

375 Vinayachandran, P. N. and Nanjundiah, R. S.: Indian Ocean sea surface salinity variations in a coupled model,  
376 *Climate Dynamics*, 33, 245-263, 2009.

377 Xie, S.-P., Annamalai, H., Schott, F. A., and McCreary Jr, J. P.: Structure and mechanisms of South Indian Ocean  
378 climate variability, *Journal of Climate*, 15, 864-878, 2002.

379 Yokoi, T., Tozuka, T., and Yamagata, T.: Seasonal and interannual variations of the SST above the Seychelles  
380 Dome, *Journal of Climate*, 25, 800-814, 2012.

381 Yokoi, T., Tozuka, T., and Yamagata, T.: Seasonal variation of the Seychelles Dome, *Journal of Climate*, 21, 3740-  
382 3754, 2008.

383 Yu, W., Xiang, B., Liu, L., and Liu, N.: Understanding the origins of interannual thermocline variations in the  
384 tropical Indian Ocean, *Geophysical research letters*, 32, 2005.

385 Zhang, Y., Du, Y., Zheng, S., Yang, Y., and Cheng, X.: Impact of Indian Ocean Dipole on the salinity budget in the  
386 equatorial Indian Ocean, *Journal of Geophysical Research: Oceans*, 118, 4911-4923, 2013.

387 Zhang, N., Feng, M., Du, Y., Lan, J., and Wijffels, S. E.: Seasonal and interannual variations of mixed layer salinity  
388 in the southeast tropical Indian Ocean, *Journal of Geophysical Research: Oceans*, 121, 4716-4731, 2016.

389 Zhang, Q. and Yang, S.: Seasonal phase-locking of peak events in the eastern Indian Ocean, *Advances in*  
390 *Atmospheric Sciences*, 24, 781-798, 2007.

391 Zhang, Y. and Du, Y.: Seasonal variability of salinity budget and water exchange in the northern Indian Ocean  
392 from HYCOM assimilation, *Chinese Journal of Oceanology and Limnology*, 30, 1082-1092, 2012.

393

394

395 **Table 1**

396 **List of positive IOD events and negative IOD events in our study period.**

pIOD years	1982	1983	1994	1997	2006	2012	2015
nIOD years	1981	1989	1992	1996	1998	2010	2014

397

398 **Table 2**

399 **List of El Niño events and La Nina events in our study period.**

El Niño years	1982	1987	1991	1997		
La Nina years	1988	1998	1999	2007	2010	

400

401

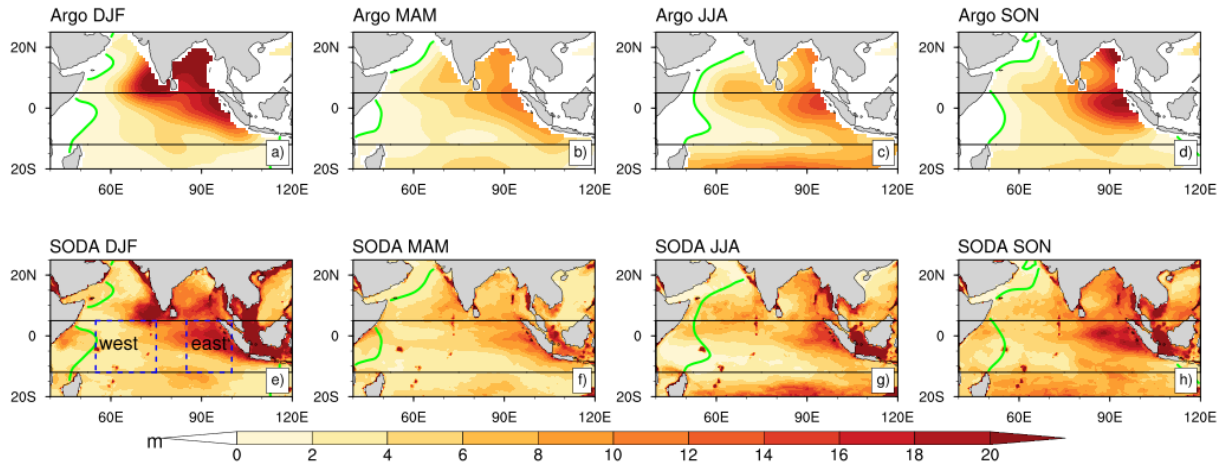
402

403

404

### BLT (2005-2015)

405

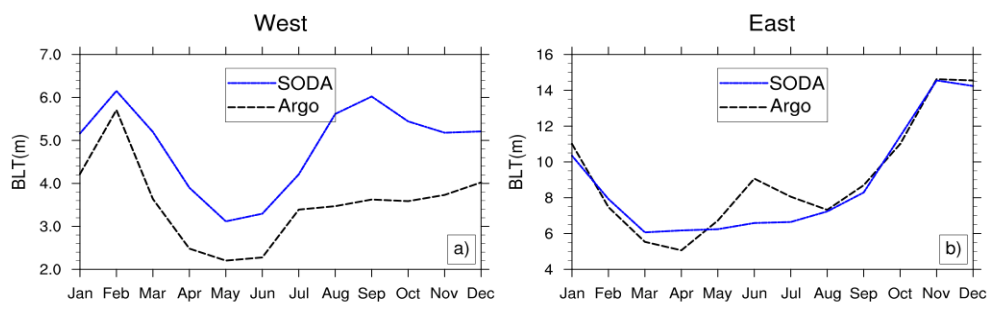


406

407 **Figure 1. Seasonal distributions of the BLT climatology obtained from Argo (a) and SODA (b) from 2005 to 2015 in**  
408 **the Indian Ocean. Units: m. The thicker green line is the zero BLT line from Argo and the dashed blue lines represent**  
409 **the areas of the western TIO (55°E-75°E, 5°N -12°S) and the eastern TIO (85°E-100°E, 5°N -12°S), respectively. The**  
410 **two thin black lines represent the latitudes of 12°S and 5°N, respectively.**

411

412



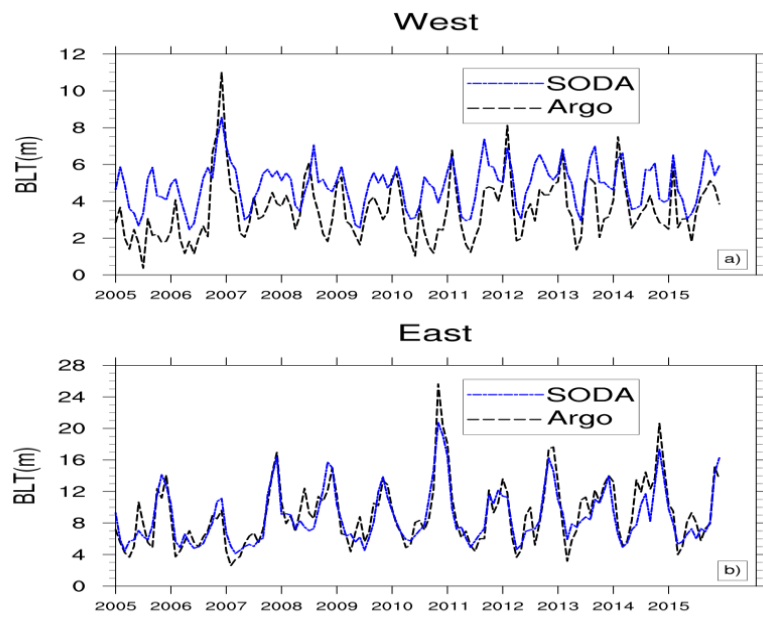
413

414 **Figure 2. Seasonal cycle of the region-averaged BLT for SODA and Argo: a) the western TIO (55°E- 75 °E, 12°S-**

415 **5°N), and b) the eastern TIO ( 85°E - 100 °E, 12°S - 5°N).**

416

417

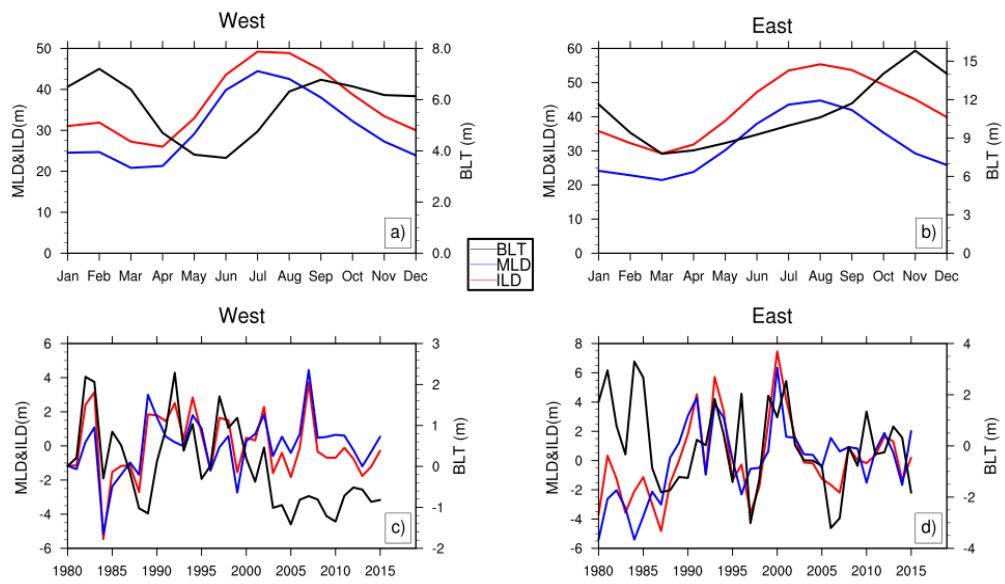


418

419 **Figure 3. Interannual time series of the region-averaged BLT for SODA and Argo: a) the western TIO (55°E- 75 °E,**  
420 **12°S- 5°N), and b) the eastern TIO ( 85°E - 100 °E, 12°S - 5°N).**

421

422



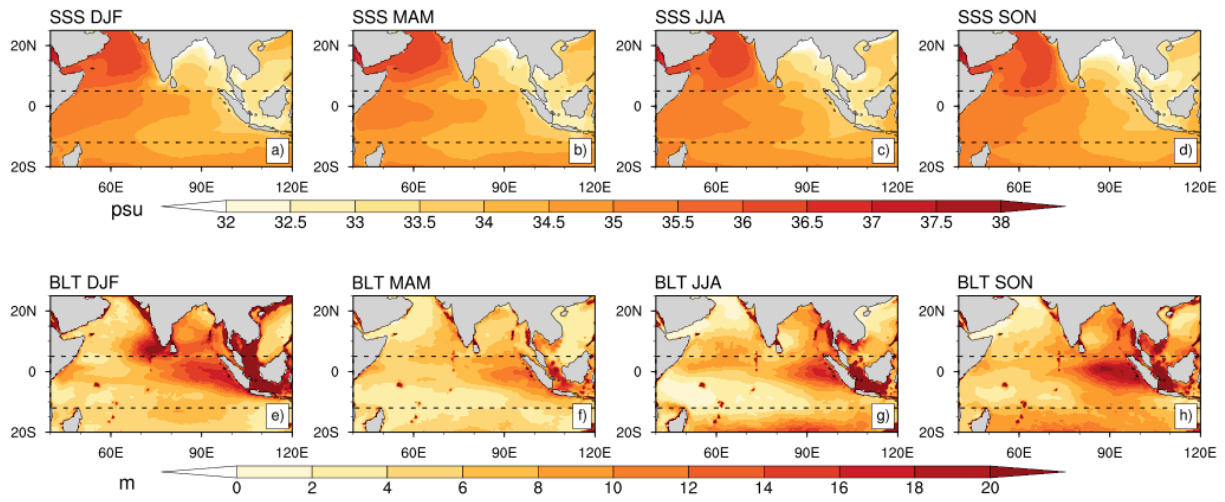
423

424 **Figure 4. The seasonal and interannual variations of BLT, MLD and ILD : a,c) the western TIO (55°E- 75 °E, 12°S-**  
425 **5°N), and b,d) the eastern TIO ( 85°E - 100 °E, 12°S - 5°N).**

426

427

(1980-2015)



428

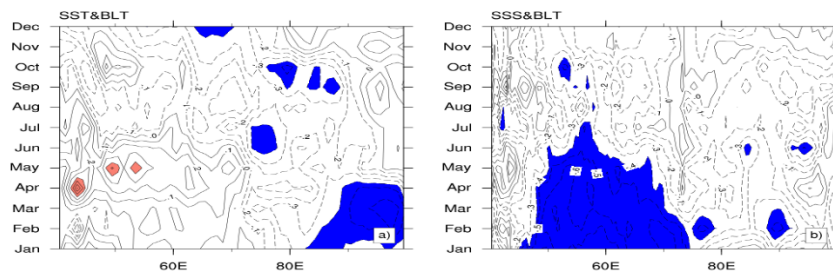
429

430 **Figure 5. The seasonal distributions of SSS (unit: psu; a-d) and BLT (unit: m; e-h) in the Indian Ocean from 1980 to**  
431 **2015. The two dashed black lines represent the latitudes of 12°S and 5°N, respectively.**

432



433

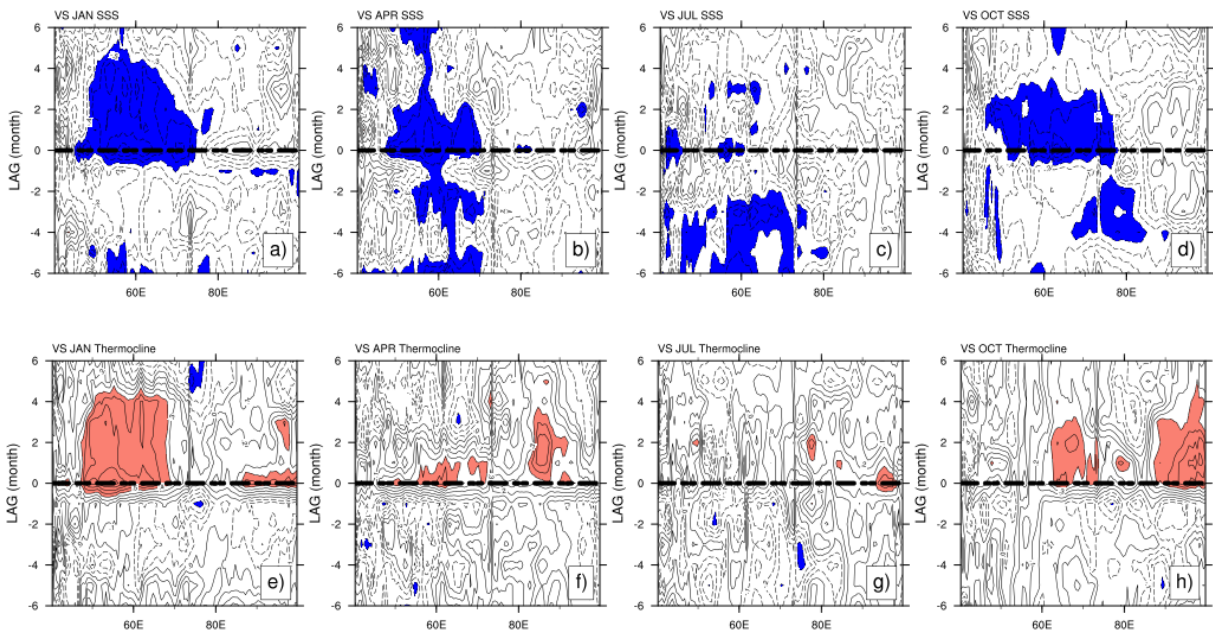


434

435 **Figure 6. Simultaneous correlations along the area of  $(12^{\circ}\text{S}-5^{\circ}\text{N})$  for (a) SST and (b) SSS anomalies with respect to**  
436 **BLT anomalies. Shaded areas exceed the 95% significance level, while the red and blue shaded areas represent the**  
437 **areas with the positive and negative correlation coefficients, respectively.**

438

439



440

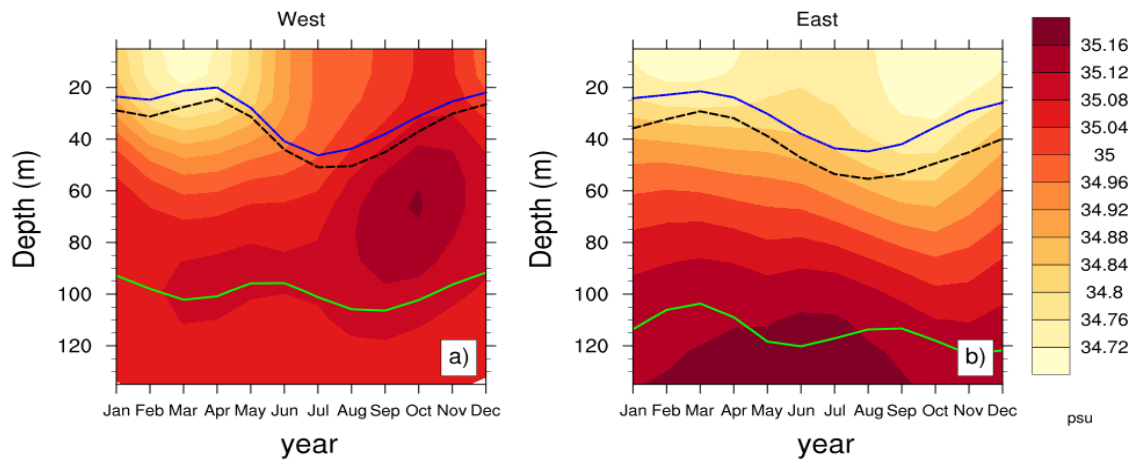
441

442 **Figure 7. Lead – lag crossing correlations of BLT with SSS (a-d) and thermocline(e-h) anomalies for January (JAN),**  
443 **April (APR), July (JUL), and October (OCT) along the area of (12°S-5°N) from 1980 to 2015. Shaded areas exceed the**  
444 **95% significance level. Positive lag means SSS (thermocline) leads BLT, and vice versa. Blue (red) shaded areas**  
445 **represent the negative (positive) correlation. The thick black dashed line represents the in-phase correlation.**

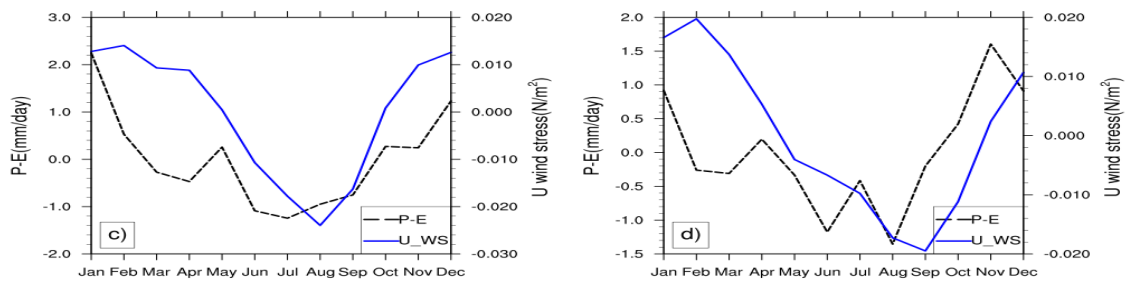
446

447

448



449



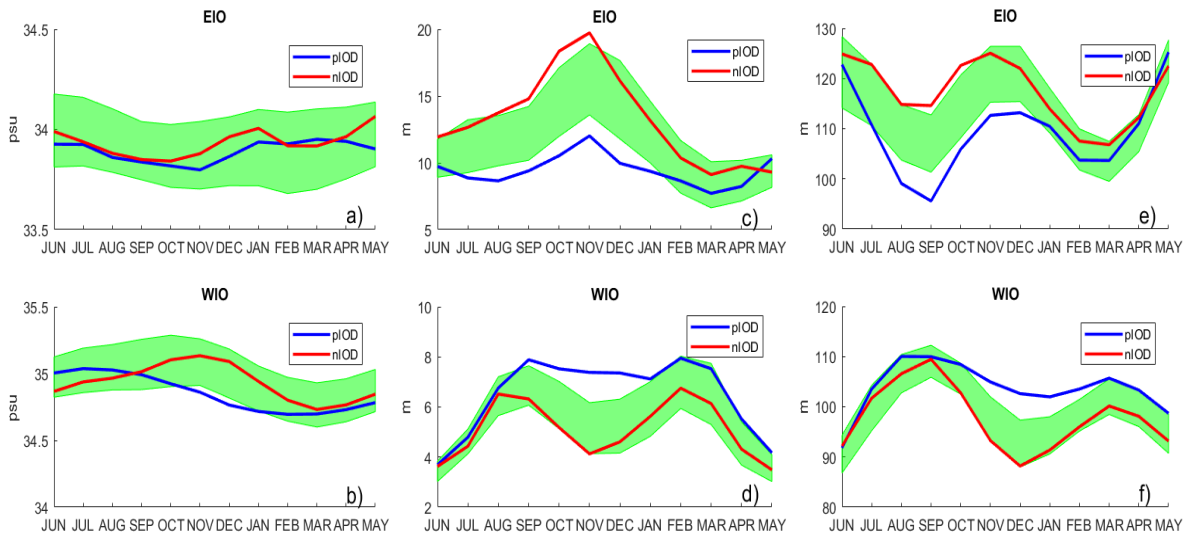
450

451 **Figure 8. Seasonal variation in the western TIO (12°S-5°N, 55°E-75°E) (a,c) and the eastern TIO (12°S-5°N, 85°E-**  
452 **100°E) (b,d). The top figures show the depth-time plots of the upper-ocean salinity (shaded), the thermocline depth**  
453 **(green line), isothermal layer (black dashed line) and mixed layer (blue line). The bottom figures show the freshwater**  
454 **flux (P-E) and zonal component of the wind stress (U\_WS) anomalies in the crossponding areas.**

455

456

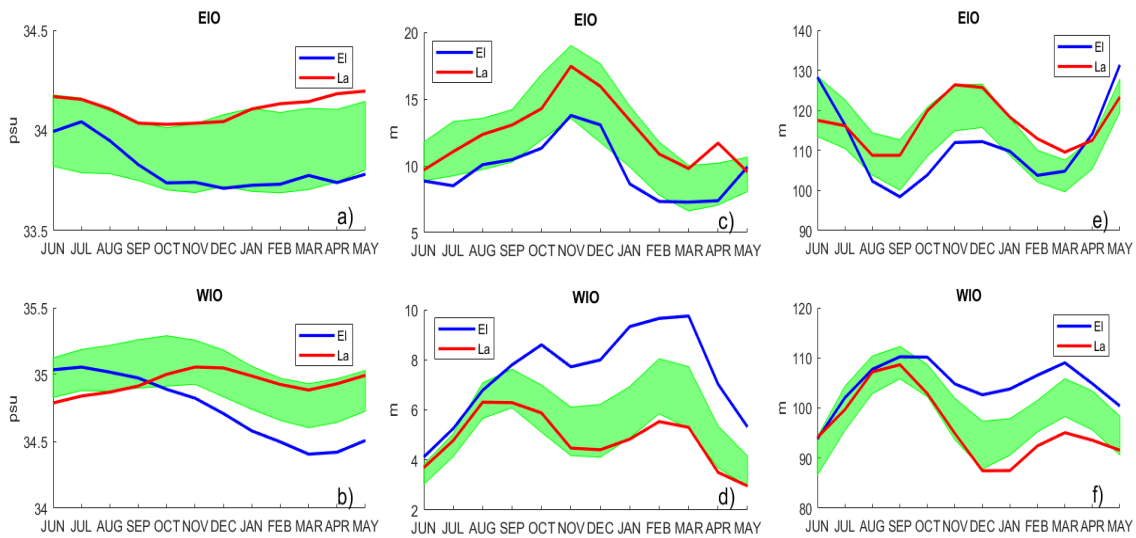
457



458

459 **Figure 9. The compositing seasonal variations of SSS (a, b; unit: psu), BLT (c, d; unit: m) and the thermocline**  
 460 **depth(e, f; unit: m) in the IOD events during the period of 1980-2015 averaged by the areas of the eastern TIO (EIO,**  
 461 **85°E-100°E, 12°S-5°N) and the western TIO (WIO, 55°E-75°E,12°S-5°N), separately. The blue line represents**  
 462 **composite in the positive IOD events and the red one represents that in the negative IOD events and the green shaded**  
 463 **area represents the 95% Monte-Carlo significance level.**

464

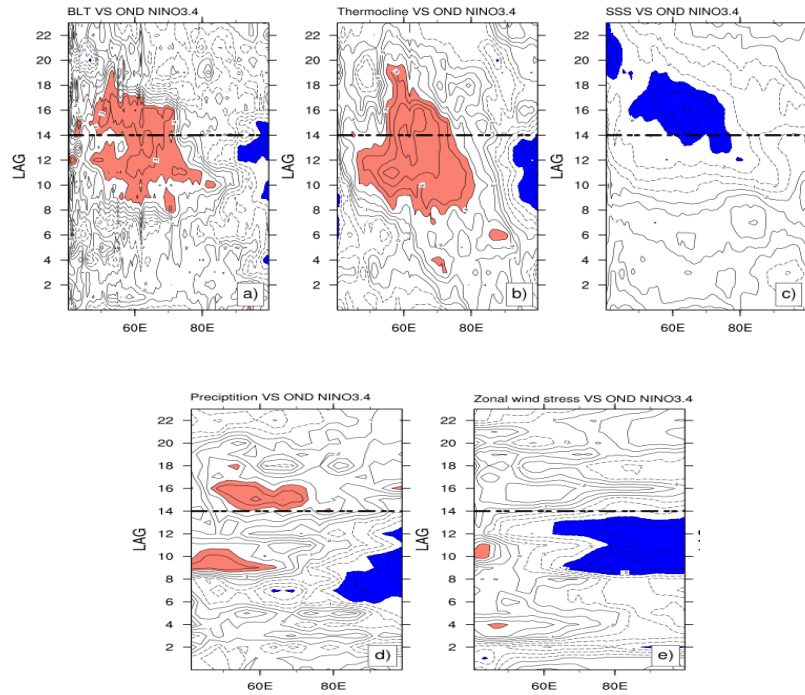


465

466 **Figure 10. Same as Figure 9 but composite in the El Niño and La Nina years.**

467

468

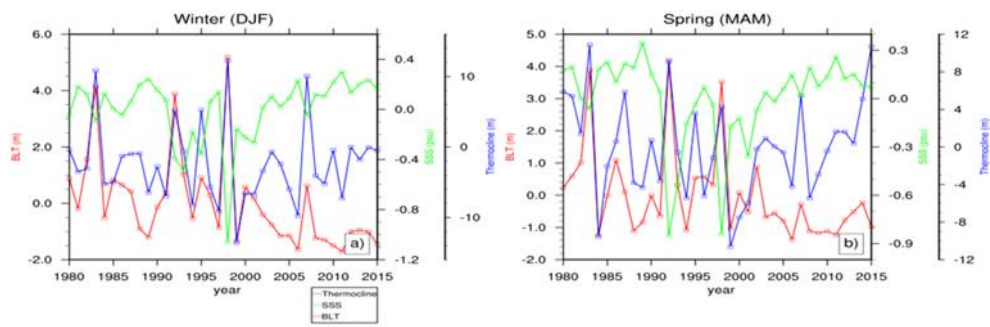


469

470 **Figure 11. Lagged correlations of (a) BLT, (b) the thermocline depth, (c) SSS, (d) precipitation, and (e) the zonal wind**  
471 **stress anomalies averaged in (12°S-5°N), with the Nino3.4 index as a function of longitude and calendar month**  
472 **(Shaded areas exceed 95% significance level; positive lagging correlations are shaded in red and negative ones are in**  
473 **blue; the thick black dashed line represents the start of the decaying phase of El Niño).**

474

475



476

477 **Figure 12. Time series of BLT, SSS and thermocline anomalies averaged over the western TIO (12°S-5°N, 55°E-75°E)**  
478 **during boreal winter (a) and spring (b) from 1980 to 2015. Red, green, and blue lines represent BLT, SSS and the**  
479 **thermocline depth, respectively.**

480

481

482

483

484

485